Int. J. Electrochem. Sci., 14 **(2019)** 6488 – 6499, doi: 1020964/2019.07.59

International Journal of ELECTROCHEMICAL SCIENCE
www.electrochemsci.org

Two-Step Approach Based on Solution Mixing and Hot Compaction for CNT/HDPE Nanocomposite Preparation

Ali Jaffal[1], *Rund Abu- Zurayk*[2,3], *Mahmoud Al-Hussein*[1,2,*]

[1] Department of Physics, The University of Jordan, Amman 11942, Jordan
[2] Nanotechnology Center, The University of Jordan, Amman 11942, Jordan
[3] Hamdi Mango Center for Scientific Research (HMCSR), The University of Jordan, Amman 11942, Jordan
[*]E-mail: m.alhussein@ju.edu.jo

Received: 12 February 2019 / *Accepted:* 8 April 2019 / *Published:* 10 June 2019

We present a simple two-step approach for preparing large uniform sheets of multi wall carbon nanotube/high density polyethylene (MWCNT/HDPE) nanocomposites. Fragmented pieces of the nanocompoite produced by solution mixing are fused into large uniform sheets using hot compaction for short time. Nanocomposite samples with CNT content of 1, 2, and 3 wt% were prepared using this approach and characterized using SEM, XRD and impedance spectroscopy. SEM images of the prepared nanocomposites illustrate homogenous dispersion of the CNTs between the PE crystalline lamellae. Crystallinity of the HDPE matrix increases with increasing the CNTs content due to their nucleating effect as revealed from the analysis of the XRD results. Impedance spectroscopy is used to determine the electrical conductivity of the nanocomposites. Nyquist plots and equivalent circuit modeling are used to extract the bulk resistance, which is in turn used to calculate the conductivity using self-developed fitting routines. Samples with only 1 wt% CNT content exhibit a conductivity of 2.3×10^{-8} S/m which increases more than 3 orders of magnitude with increasing the CNTs content due to the good dispersion and more interconnected conductive network within the HDPE matrix.

Keywords: Carbon nanotubes, High density polyethylene, Nanocomposites, Morphology, Electrical conductivity.

1. INTRODUCTION

Carbon nanotube (CNT) polymer nanocomposites are a class of high-performance materials for many novel applications [1-5]. The properties of these nanocomposites depend on the nature of the polymer matrix and the preparation method. An appropriate preparation method must ensure a uniform dispersion of the nanotubes into the polymer matrix without destroying their structural integrity. To this end, several methods have been used [6-9]. The two commonly used methods are the solution mixing and melt mixing. Each of these methods has its own advantages and disadvantages. While melt

mixing is suitable for producing large size uniform sheets, samples produced by solvent mixing have generally small sizes. Meanwhile, melt mixing requires heating above the equilibrium temperature of the polymer matrix under constant mechanical shear for a relatively long time to ensure good CNTs dispersion. These conditions might destroy the structure integrity of the CNTs thus undermining the properties of the resulting nanocomposite. By contrast, solvent mixing is performed under less stringent conditions for the CNTs. Therefore, it is desirable to find a strategy for the preparation of nanocomposites that combines the advantages of both methods. In this work, we report a two-step approach based on these two methods that is capable of producing large nanocompsite samples. In the first step, solution mixing is used to disperse the CNTs in the polymer matrix. In the second step, the small pieces produced after drying the solvent are fused together using hot compaction for a short period of time [10]. We demonstrate this two-step approach through the preparation and characterization of the morphology and electrical conductivity of nanocomposites based on multi wall carbon nanotubes (MWCNTs) dispersed in a linear high density polyethylene (HDPE) having CNTs content of 1, 2 and 3 wt.%.

2. EXPERIMENTAL

2.1. Materials and Nanocomposite Preparation

The HDPE pellets, the MWCNTs and all solvents used in this study were purchased from Sigma-Aldrich. The MWCNTs were treated prior to their incorporation into the HDPE matrix in order to functionalize their surfaces with carboxyl groups. 0.4 g of CNTs were first put in a flask containing 100 ml of sulfuric acid (98%) and nitric acid (70%) (v/v 1:3). The resulting mixture was then sonicated with an ultrasonicator at room temperature under reflux at 120 °C for two hours. After that the CNTs were filtered through 0.45 μm pore size cellulose membrane and washed with deionized water to remove the acid residues until the pH was 7. Then they were dried in a vacuum oven at 100 °C for one hour.

A two-step approach was used to prepare nanocomposites of CNT/HDPE. In the first step, the treated CNTs and HDPE pellets were dispersed in Xylene. After two hours of sonication, the solution was left to dry for two days rendering small fragmented pieces of the nanocomposites. In the second step hot compaction was used to fuse these small pieces into large uniform sheets as follows. The small pieces produced in the first step were placed between two aluminium plates (15 cm × 15 cm) in a heated press at 160 °C. A small contact pressure was applied to the plates first then a higher pressure of 4450 Pa was applied for a couple of minutes. After that the plates were removed from the press and put directly into a water bath at room temperature. Three CNTs/HDPE nanocomposites with 1, 2, and 3, wt% of carbon nanotubes were prepared. A pure HDPE sample was also prepared using the two-step approach in order to be taken as a reference. Table 1 lists all prepared samples.

Table 1. The prepared samples using the two-step approach.

Sample	MWCNT (wt%)
S_1	0
S_2	1
S_3	2
S_4	3

2.3 Nanocomposite Charecterization

The morphology of the prepared nanocomposites and the dispersion of the CNTs within the HDPE matrix were characterized by high resolution field emmision scanning electron microscopy (Bruker FEI-Inspect F50). The crystalline structure of the HDPE matrix was determined by X-ray diffraction (XRD-6000, Shimadzu, Japan) using Cu-Kα radiation (λ = 0.15406 nm at 40 kV and 30 mA) in the range of 10 – 30˚ for 2θ, with a scanning speed of 2˚/min. A Solartron 1260 Impedance/Gain-phase analyzer was used to perform AC impedance measurements, in a frequency range of 1 to 10 ^{6} Hz, at room temperature with 0.3 V DC bias voltage.

The measured impedance modulus $|Z|$ and phase angle ϕ as a function of frequency were used to calculate the real and imaginary components of the complex impedance Z' and Z'', respectively. The extracted data were then presented as Nyquist plots [11-14]. Equivalent circuit models were used to estimate the bulk resistance, *R*, of the nanocomposites. The conductivity (σ) of the nanocomposites was then calculated using:

$$\sigma = \frac{L}{RA} \quad \text{.....(1)}$$

where *L* corresponds to the thickness of the sample, and *A* is the area of the electrodes.

3. RESULTS AND DISCUSSION

3.1 Composite Preparation

The hydrophobic nature of MWCNTs drives them to agglomerate into dense bundles rendering them insoluble in most organic solvents. The oxidation procedure with nitric acid and sulfuric acid is expected to add carboxyl groups (COOH) at the walls of the MWCNTs. This surface modification reduces the hydrophobicity of the MWCNTs and enhances their solubility and compatibility with the polymer matrix [9]. Figure 1 shows an SEM image of the treated MWCNTs.

Figure 2(a) shows a typical photograph of the nanocomposite sheets produced after the solution mixing step of S_4 sample. As can be seen, fragmented small pieces are produced. Such sheets are not suitable for some characterization techniques such as mechanical and electrical characterizations. More importantly, uniform large sheets are required for many practical applications. To achieve this, we used a hot compaction method as explained in the experimental section. Figure 2(b) shows a typical

sheet produced after the hot compaction step for the same S_4 sample. As can be seen, large isotropic sheets are now produced. It is important to note that during the hot compaction step, high temperatures, high pressures or long waiting time in the heated press under pressure should be avoided as this might destroy the CNTs integrity leading to nanocomposutes with inferior properties. The idea is to perform the hot compaction step at a temperature that is high enough to melt some regions of the polymer matrix only and not the whole sheet. The molten material will then act as a binder for the small pieces without affecting much of the naocomposite structure that was formed originally in the solution mixing step.

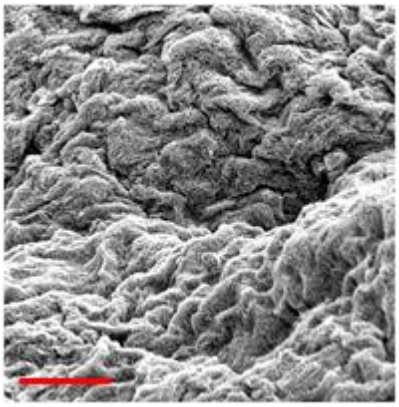

Figure 1. SEM image of MWCNTs treated in sulfuric acid and nitric acid prior to their incorporation into the HDPE matrix in order to functionalize their surfaces with carboxyl groups. The bar size is 5 μm.

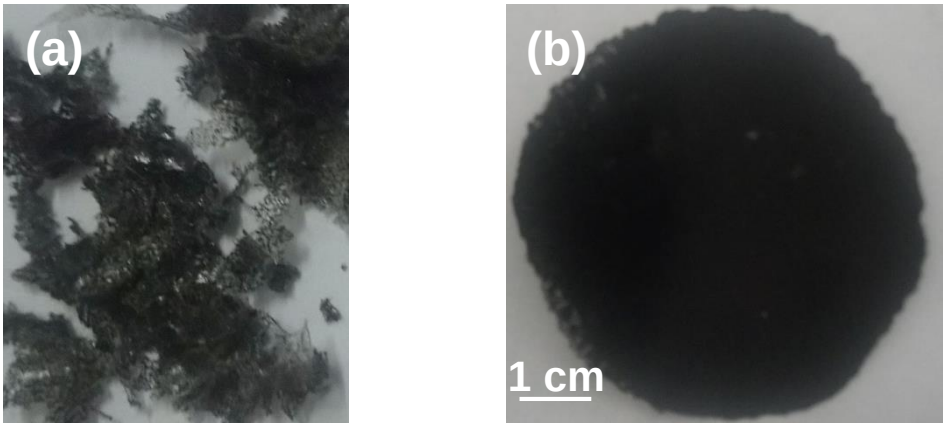

Figure 2. Photographs of the S_4 nanocomposite produced after (a) solution mixing step, and (b) hot compaction step at 160 °C for a couple of minutes.

3.2 Structure and Morphology:

SEM was used to probe the morphology and the CNTs dispersion of the prepared samples. Figure 2 shows SEM images of all samples. The HDPE sample exhibits typical lamellar crystalline

structure with lamellae having an edge-one orientation appear brighter. As a general observation, the images of all nanocomposite samples show that large agglomerations of CNTs are not observed indicating a homogeneous dispersion of the CNTs between the PE lamellae.

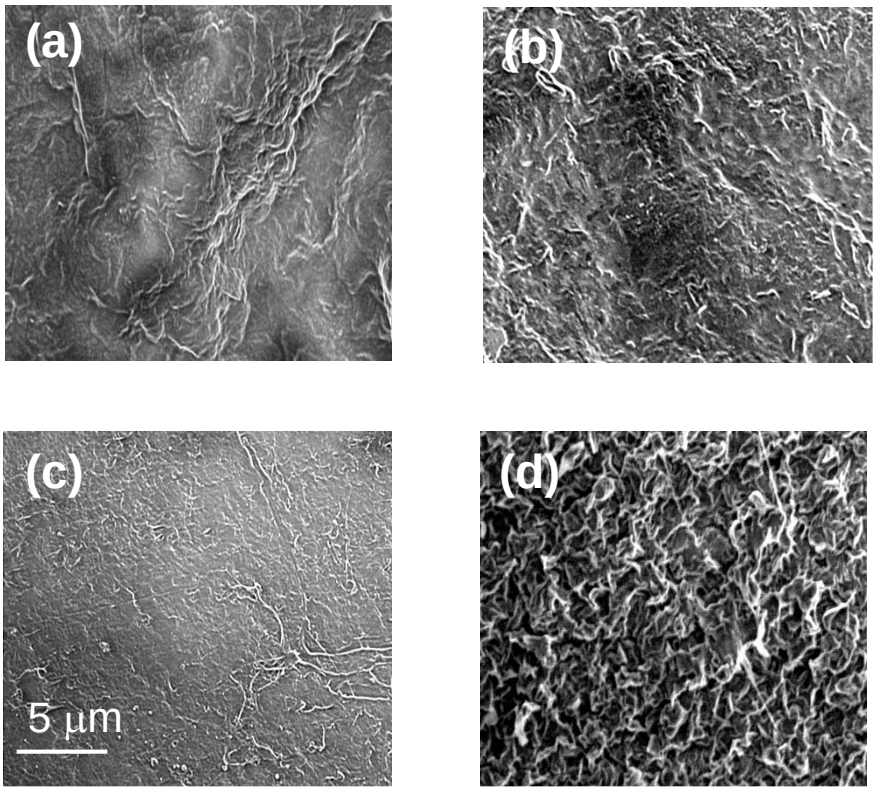

Figure 3. SEM images of (a) S_1, (b) S_2, (c) S_3 and (d) S_4 prepared using the two-step approach.

It is known that PE is a semicrystalline polymer [15-17]. XRD was used to investigate the crystalline structure and in particular how the crystallinity of the HDPE matrix varies with the CNTs content of the nanocomposites. Figure 4 shows XRD curves of all samples. All samples exhibit two relatively sharp reflections, (110) and (200), typical of the PE orthorhombic crystalline structure superimposed on a broad amorphous halo. However, the peak intensities and full width at half maximum (FWHM) of the (110) and (200) reflections vary among the different samples. Curve fitting was used to extract the peak position, FWHM, and peak intensity of all reflections. Each peak was fit to a Gaussian function.

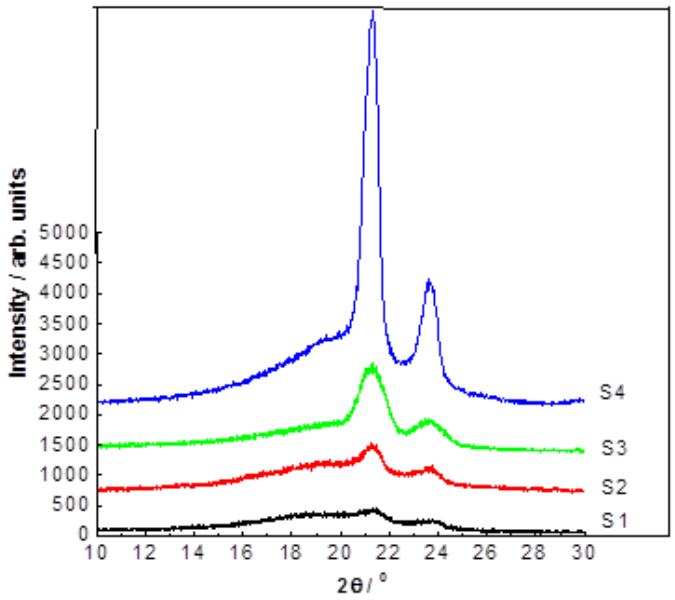

Figure 4. XRD curves of all prepared samples. The curves are shifted vertically for clarity.

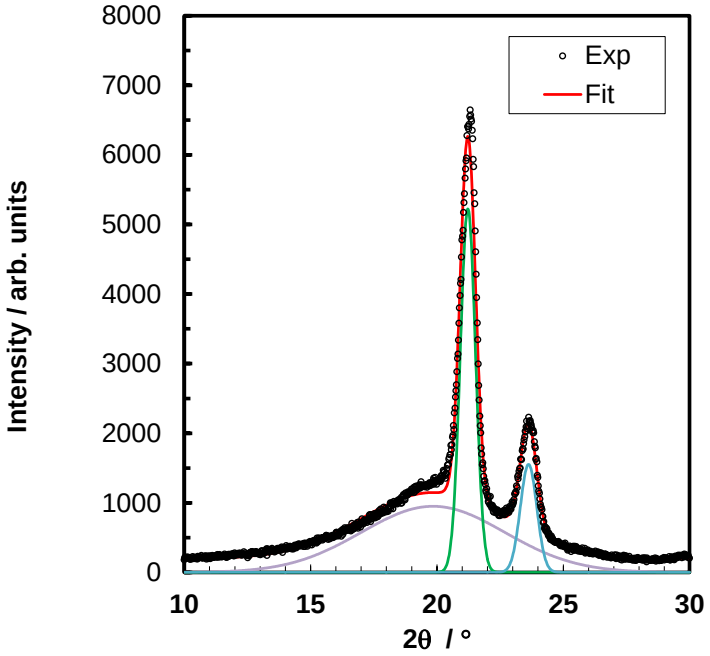

Figure 5. XRD curve of the S_4 sample fit with three Gaussian functions in addition to a constant background. The fit curves appear as solid lines.

The sum of the three Gaussian functions and a constant background was used to fit the whole curve. Figure 5 shows a typical fit for the S_4 sample. The (110), (200) and the amorphous peaks are centered at 2θ of 21.3°, 23.7° and 19.8°, respectively.

After resolving all reflections, the crystallinity, χ, was calculated by dividing the total area of the (110) and (200) peaks by the total area under the XRD diffraction curve (crystalline plus amorphous peaks). The results are summarized in Table 2. For pure HDPE, the crystallinity was only 11%. It is known that HDPE exhibits higher values of crystallinity under suitable preparation conditions. This low value of crystallinity indicates that the preparation conditions were far from being optimum for HDPE crystallization. We attribute this to the fast kinetics of the preparation that suppresses crystallization due the fast cooling after removing from the press into the water bath.

Table 2. The calculated crystallinity of prepared samples.

Sample	χ (%)
S_1	11
S_2	14
S_3	40
S_4	46

It is observed that the crystallinity increases with increasing the CNT content. The substantial increase of crystallinity of HDPE (46 % for S_4) suggests that CNT can provide nucleation sites at their surfaces for the crystallization of the HDPE (heterogeneous nucleation) [15].

3.3 Impedance and Conductivity

Figure 6 shows the real part of the impedance as a function of frequency for all samples. The HDPE sample exhibits a typical behaviour of an insulating material. In contrast, all nanocomposite samples exhibit similar features. At low frequency, Z' exhibits resistive behaviour (frequency-independent), whereas at high frequency it exhibits capacitive behaviour (frequency-dependent) behaviour. It is worth noting that this behaviour is observed with CNTs content of only 1 wt%. This indicates that a good dispersion of the CNTs within the polymer matrix is attained using this two-step approach even for low CNTs content. It is also worth noting that the frequency range of the resistive behaviour increases with increasing the CNTs content due to more interconnected CNT network. The improved connectivity of the conductive pathways in the nanocomposite leads to higher electrical conductivity of the nanocomposites. At very high frequencies, the Z' curves merged together indicating the absence of interfacial polarization at these frequencies.

Figure 7 shows Nyquist plots (representations of Z'' versus Z' on a normal scale plot) for all nanocomposite samples. A semicircle shape is observed for all samples indicating the presence of polarization with a single relaxation time [14]. This suggests a homogeneous structure of the nanocomposites in agreement with the SEM results. The peak and radius of the semicircle decreased with the increase in MWCNT content, i.e., decrease in the nanocomposite resistivity. To extract the bulk resistance and other parameters related to the conduction mechanism, we fit these plots using equivalent circuit models. Many models can be used for such fitting [14]. The simplest one is the RC-parallel model illustrated in Figure 8(a). It consists of a resistor corresponding to the bulk resistance, *R*, and a capacitor, *C*, that represents polarization relaxations [15]. The real and imaginary components of the equivalent impedance of this model at a certain frequency *f* are given by:

$$Z' = \frac{\mathrm{R}}{(1+4\pi^2 f^2 R^2 C^2)} \text{.....(2)}$$

$$Z'' = -\frac{2\pi f C R^2}{(1+4\pi^2 f^2 R^2 C^2)} \text{. .....(3)}$$

The parameters of the equivalent circuit model are estimated for each sample using self-developed routines using a non-linear least square procedure that minimizes χ^2 function for each frequency as defined by:

$$\chi^2 = \sum_{i=1}^{n} \frac{|z'_{exp}(f_i) - z'_{the}(f_i)|^2}{|z'_{exp}(f_i)|^2} + \frac{|z''_{exp}(f_i) - z''_{the}(f_i)|^2}{|z''_{exp}(f_i)|^2} \text{.....(4)}$$

where $z'_{exp}(f_i)$, $z''_{exp}(f_i)$, $z'_{the}(f_i)$ and $z''_{the}(f_i)$ denote the experimental and model components of the impedance, respectively, f_i the frequency of measurement *i*.

A better fit was obtained by replacing the capacitor by a constant phase element (CPE), Figure 8(b), to take into account the nonideality of the capacitor. For this model, the real and imaginary components of the equivalent impedance of this model can be written as:

$$Z' = \frac{R(1+R(2\pi fC)^n \cos\left(\frac{n\pi}{2}\right))}{1+2R(2\pi fC)^n \cos\left(\frac{n\pi}{2}\right)+(R(2\pi fC)^n)^2} \text{.....(5)}$$

$$Z'' = -\frac{R^2(Cf)^n \sin(\frac{n\pi}{2})}{1+2R(2\pi fC)^n \cos\left(\frac{n\pi}{2}\right)+(R(2\pi fC)^n)^2} \text{.....(6)}$$

where n is the exponent of CPE or depressing factor ($0 < n \leq 1$); $n = 1$ for an ideal capacitor. Figure 9 shows the fit obtained using this modified RC-model. The extracted parameters are listed in Table 3 for all nanocomposite samples. The conductivity values calculated using *R* values obtained from the fit are also listed in Table 3. As can been seen, σ increases with increasing CNT content reaching a value of 9.08×10^{-6} S/m for the nanocomposite having 3 wt% CNT content. This is more than three orders of magnitude higher than that of the 1 wt% CNT nanocomposite indicating that more connected paths ways are formed with increasing CNT content. This is comparable with reported values in the literature for similar CNT/HDPE nanocomposites [19, 20].

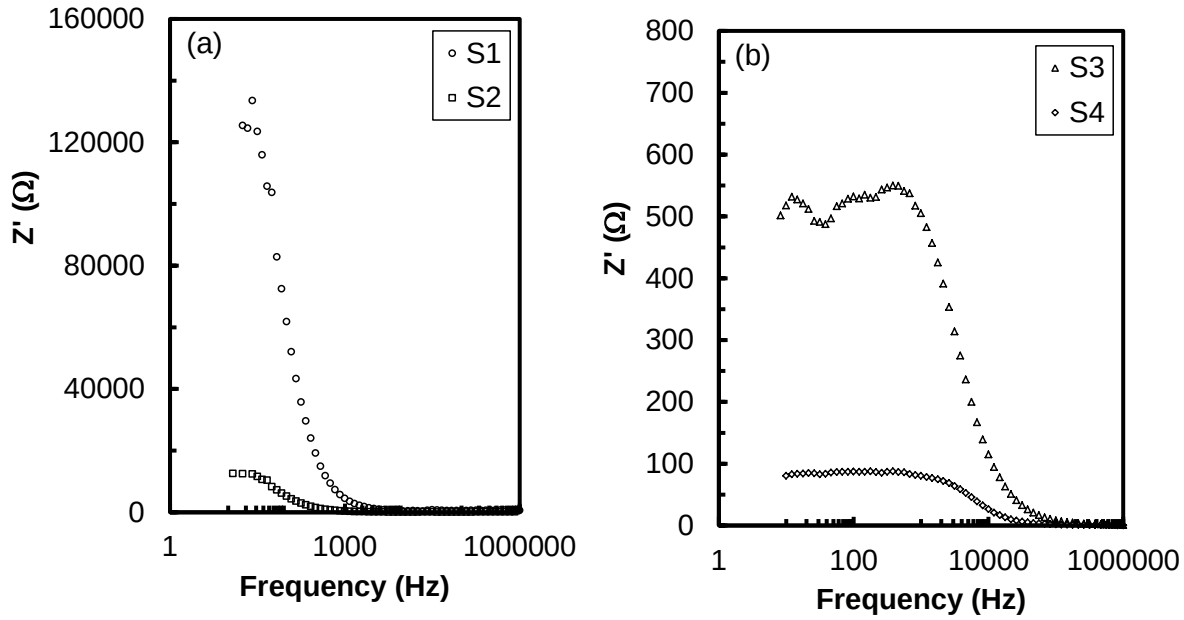

Figure 6. Real component of the impedance as a function of frequency for all samples.

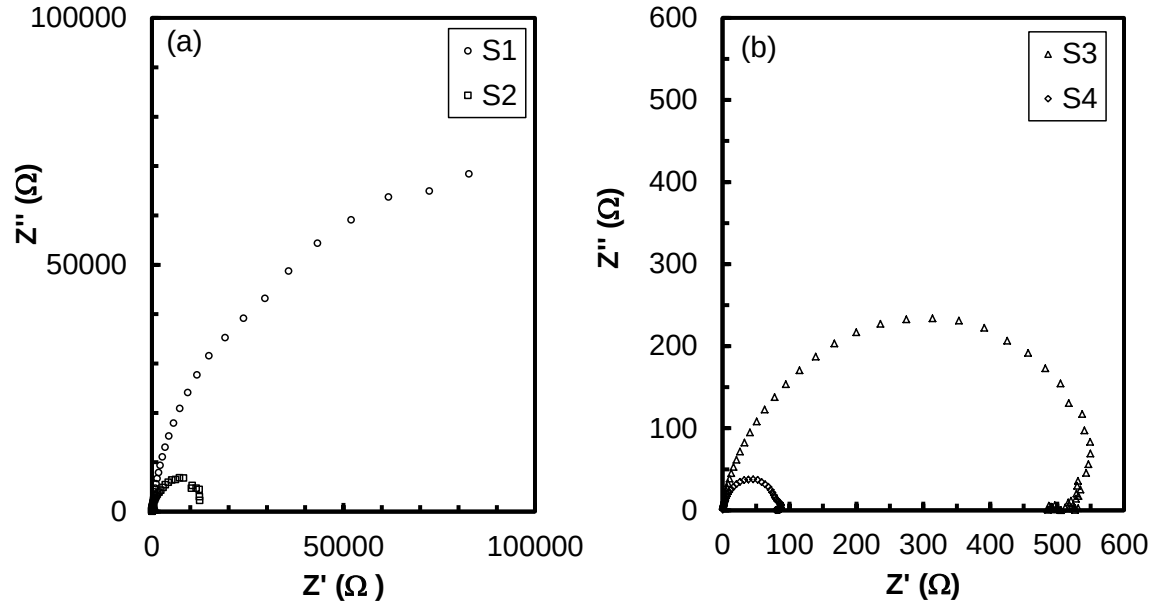

Figure 7. Nyquist plots for all samples of the data presented in Figure 5 for all samples.

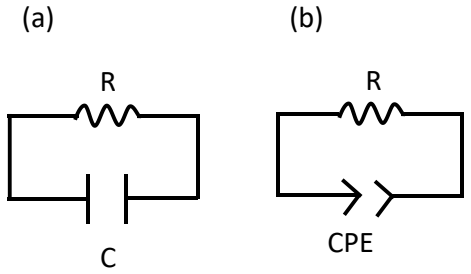

Figure 8. Equivalent circuit models used to fit the impedance response of the nanocomposites. (a) RC-parallel model and (b) modified RC-parallel model.

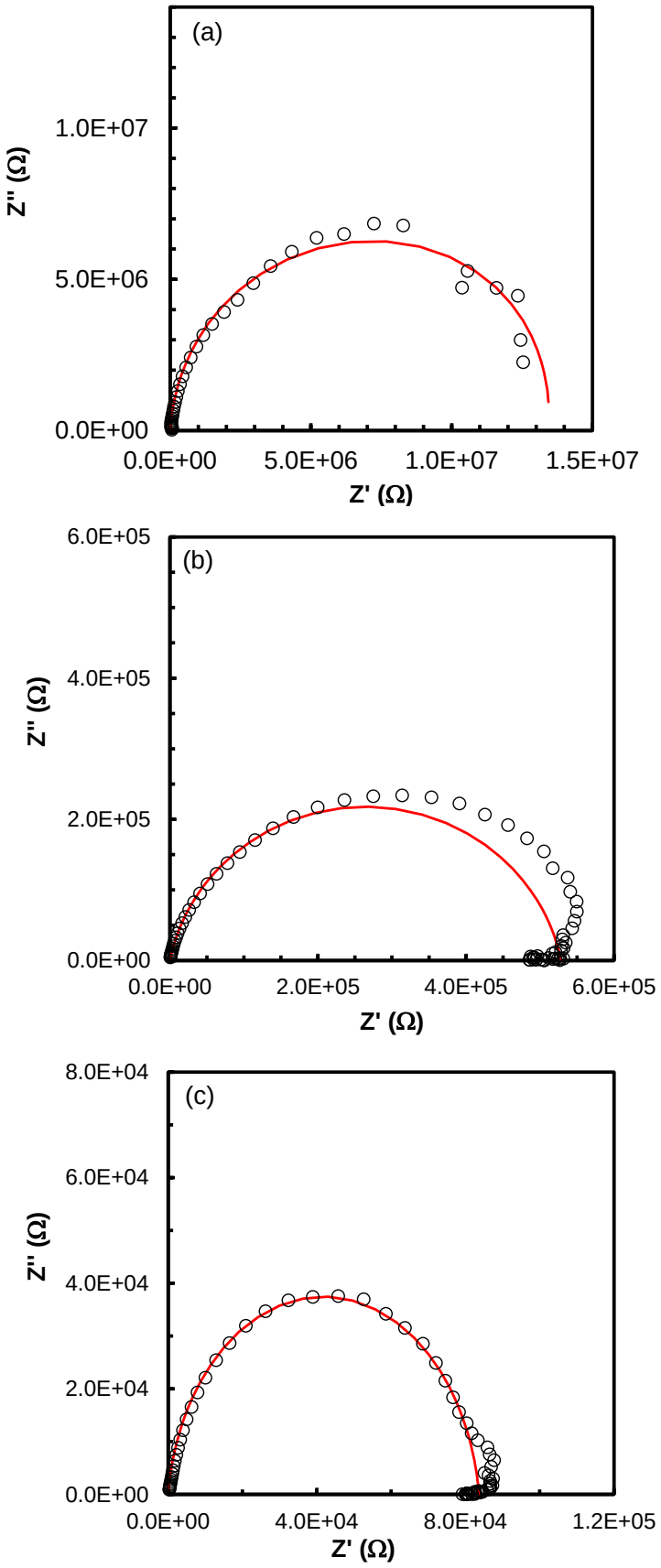

Figure 9. Nyquist plots for all nanocomposite samples. The solid lines represent the best fit obtained using the modified RC-parallel model. (a) S_2 sample, (b) S_3 sample and (c) S_4 sample.

Table 3. The extracted parameters from the modified RC-parallel model for all nanocomposite samples.

Sample	R ($\times 10^4\ \Omega$)	n	C ($\times 10^{-11}$ F)	σ ($\times 10^{-6}$ S/m)
S_2	1.34×10^3	0.96	18.1	0.023
S_3	52.84	0.88	24.4	3.590
S_4	8.36	0.93	59.7	9.080

4. CONCLUSIONS

Large uniform MWCNT/HDPE nanocomposite sheets suitable for practical applications were prepared using solution mixing followed by hot compaction for a short time. This two-step approach provides a facile means to prepare large sheets of nanocomposites out of fragmented small pieces obtained frequently using solution mixing method. The compaction temperature should be high enough to melt only some of the fragmented sheets. The molten regions act as a glue that binds the small pieces without affecting their original structure. The structure, morphology and electrical conductivity of the prepared samples were also characterized. The results revealed that good dispersion of the CNTs between the HDPE crystalline lamellae was achieved. A substantial increase in the electrical conductivity was also achieved even with low CNT content of 1 wt%.

ACKNOWLEDGEMENTS
The financial support of The University of Jordan is gratefully acknowledged. We thank Ms. Rula Albuqain and Mr. Yousef AbuSalhah for their assistance in performing the SEM and XRD measurements.

References

1. E.T. Thostenson, Z. Ren and T.W Chou, *Composites Science and Technology*, 61 (2001) 1899.
2. R.H. Baughman, A.A. Zakhidov and W.A. De Heer, *Science*, 297 (2002) 787.
3. M. Moniruzzaman and K.I. Winey, *Macromolecules*, 39 (2006) 5194.
4. Y. Li, X. Huang, L. Zeng, R. Li, H. Tian, X. Fu, Y. Wang and W-H Zhong, *J. Mater. Sci.*, 54 (2019) 1036.
5. B.K. Kuila, K. Park and L. Dai, *Macromolecules*, 43 (2010) 6699.
6. P. Potschke, T.D. Formes and D.R. Paul, *Polymer*, 43 (2002) 3247.
7. K.T. Lau and D. Hui, *Carbon*, 40 (2002) 1605.
8. W. Tang, M.H. Santare and S.G. Advani, *Carbon*, 41 (2003) 2779.
9. S. Kanagaraj, F.R. Varanda, T.V. Zhiltsova, M.S.A. Oliveira and J.A.O. Simoes, *Composites Science and Technology*, 67 (2007) 3071.

10. I.M. Ward and P.J. Hine, *Polymer*, 45 (2004) 1413.
11. P.M. Gomadam and J.W. Weidnern, "*Analysis of electrochemical impedance spectroscopy in proton exchange membrane fuel cells"*, Wiley, USA (2005).
12. F. Kremer, A. Schonhals and W. Luck, "*Broadband dielectric spectroscopy"*, Springer Velarg-Berlin, Heidelberg, New York (2002).
13. X. Yuan, H. Wang, J.C Sun and J. Zhang, *Int. J. Hydrogen Energy*, 32 (2007) 4365.
14. X-Z Yuan, C. Song, H. Wang and J. Zhang, "*Electrochemical impedance spectroscopy in pem fuel cells: Fundamentals and applications*", Springer, London (2010).
15. G. Strobl, *The Physics of Polymers*; Springer: Berlin (1996).
16. M. Al-Hussein, G.R. Davies and I.M. Ward, *Polymer*, 42 (2001) 3679.
17. M. Al-Hussein, G.R. Davies and I. M. Ward, *J. Polym. Sci. B: Polym. Phys.*, 38 (2000) 755.
18. G. Al-Madani, M.H. Kailani, M. Al-Hussein, *Int. J. Electrochem. Sci*., 10 (2015) 6465.
19. J. Du, L. Zhao, Y. Zeng, L. Zhang, F. Li, P. Liu and Ch. Liu, *Carbon*, 49 (2011) 1094.
20. X. He, Zh. Ying, J. Du, X. Tong and H.-M. Cheng, *The American Carbon Society*, (2004) E017.